# A new function for the optimal placement of piezoelectric plates to control multimode vibrations of a rotating beam

F. Botta[1,#], D. Dini[2,*], R. de Lieto Vollaro[3,#]

[#] Dipartimento di Ingegneria – Universita' degli Studi Roma Tre, Via della Vasca Navale, 79 - 00146 - Roma - Italy

[1] fabio.botta@uniroma3.it

[3] roberto.delietovollaro@uniroma3.it

[*] Department of Mechanical Engineering - Imperial College London, Exhibition Road, London SW7 2AZ

[2] d.dini@imperial.ac.uk

***Abstract*— Damping of vibrations is often required to improve both the performances and the integrity of engi-engineering structures, e.g. gas turbine blades. In [24] some of the authors have proposed a new function to control the multimode vibrations of a fixed beam. In this article this methodology has been extended to a rotating cantilever beam. To develop an effective control strategy, and optimize the placement of the active piezoelectric elements in terms of vibrations amplitude reduction, a procedure has been developed and a new analytical solution has been pro-proposed. The results obtained have been corroborated by comparison with the results from a multi-physics finite elements package (COMSOL) and data from other models available in the literature.**

**Keyword: Smart materials, Piezoelectric material, Active control, Vibrations, Blades.**

**Nomenclature**

| | | | |
|---|---|---|---|
| $a$ | axis position of the centre of the piezo plates | $R$ | radius of the hub |
| **B** | vector control | $S_b$ | cross sectional area of the beam |
| $c$ | beam width | $T_a$ | piezoelectric thickness |
| **C** | damping matrix | $T_b$ | beam thickness |
| $d_{31}$ | piezoelectric coefficient | $u$ | axial displacement |
| $E_a$ | Young's modulus of the piezoelectric material | $V$ | voltage applied to the piezoelectric plates |
| $E_b$ | Young's modulus of the beam material | $w$ | vertical displacement |
| $h$ | piezo plates length | $x$ | beam axial coordinate |
| $I_b$ | inertia moment of the beam | $X_i(t)$ | amplitude of the i-th mode |
| **K** | stiffness matrix | $\alpha, \beta$ | damping coefficients |
| $L_b$ | beam length | $\xi$ | beam axial coordinate of the terminations of the PZT plates |
| $M_a$ | piezoelectric bending moment | $\overline{\xi}$ | dimensionless $\xi$: $\overline{\xi} = \xi / L_b$ |
| $n$ | revolutions per minute | $\rho$ | density |

| | | | |
|---|---|---|---|
| **M** | mass matrix | $\phi_i(x)$ | i - th flexural mode of the cantilever beam |
| *r* | percentage coupling coefficient | $\omega_i$ | natural frequency |

## I. INTRODUCTION

The development of more efficient gas turbine engines have to consider the problems of the vibrations of the most sensitive components like the compressor blades. Indeed one of the changes made to design of modern gas turbine is that the compressor blades become a little thinner and, hence, slightly more efficient; however, this makes them more sensitive to externally induced vibrations. Not only is this vibration counter-productive to the overall efficiency of the components, but it also decreases the blades' lifetime by causing high cycle fatigue (HCF) and subsequent material failures ([1]-[3]). To increase the blade life passive damping systems, such as friction damping, are typically adopted. These systems are very effective but, in contrast to active damping elements, they are not able to change their characteristics depending on the system response. In the last two decades, the adoption of piezoelectric elements, has received considerable attention by many researchers for their potential applicability to different areas of mechanical, aerospace, aeronautical and civil engineering. In fact they are characterized by an interesting coupling between electrical and mechanical quantities: a deformation appears when an electric field is applied and vice versa ([4]). More recently studies about their use in blades of turbomachinery have been carried out ([5]-[10]) but only few of these concern active damping.

In particular the damping capability of piezoelectricic shunting is analysed in [5]. A bladed disk model, with eight blades and two collocated piezoceramic actuators on each blade, is modeled by Finite Elements Model (FEM). The authors have shown that it is possible to calculate the piezoelectric coupling coefficients, and the excitation force of a piezoelectric actuator, by using a static analysis with a specfied voltage applied to the pie-piezoceramic actuators. The possibility to use the piezoelectric materials for active vibration control of a two-stage, low-speed axial flow compressor has been studied by Goltz et al ([6]). A slip ring has been used to transmit both the actuation voltage and the strain gage signal. The tests have shown that the amplitude of the induced forces are enough to control the vibration amplitude in a real component. A wireless system has been used by Provenza et al. ([7]) to control the vibrations of a rotating plate. A rotating bearing was used to excite the system; the frequency of the control was identical to the excitation frequency, while the amplitude and phase was tuned to optimize the response. The results have shown the possibility to damp the 3rd bending plate vibrations. The damping performances of a passive piezoelectric damper to reduce the turbine blade vibrations has been used by Schwarzendhall et al. ([8]). The optimal position and size, with respect to the mode shape of interest, have been also investigated. A good result has been obtained with a reduction of the maximum of the frequency response function of 11.66 times compared to the reference blade. Finally, Choi et al. ([9], [10]) have shown the experimental results obtained with a system designed to control the multimode vibrations.

However, these preliminary studies did not investigate the optimal positions of the active piezoelectric damp-dampers as a function of the modes to be controlled. Considering that the effectiveness of the piezoelectric elements to damp a particular excited mode, or a multimode combination, strongly depends on their position, and that the excited modes can change during the time, the possibility of an active system to change the work-configuration of the piezo-plates can increase considerably their efficiency. In the last years the study of the optimal position of the piezoelectric elements, and their effect, on mechanical structures has received increasing attention. Typically the aim of these studies is to find the position that minimizes an objective function or maximizes the degree of modal controllability (see [11] and [12] for a review). Crawley, de Luis ([4]) studied for first the optimal position to damp a specified mode. They found that the better position for the actuators should be in regions of higher average strain. Other researcher ([13], [14]) found analogous results. For a cantilever beam Sunar and Rao ([15]), Demetriou ([16]), Bruant et al. ([17]) and Baz and Poh ([18]) have found that more effectiveness positions of the piezoelectric actuators are closer to the fixed end. An analytical model has been presented by Yang and Lee for simultaneous optimization of non-collocated ([19]), and collocated ([20]), piezoelectric sensor/actuator placement and feedback control gain. The results have shown that this procedure can avoid the instability of the structural control system. Yang et al. ([21]) have studied a simply supported beam. They found that the optimal position for the piezoelectric plates to control one specific mode is within the regions separated by the vibration nodal lines.

Barboni et al. ([22]) examined the possibility of exciting the flexural dynamics of an Euler-Bernouilli beam, according to a single mode. According to the results to excite a desired mode the actuator must be placed be-between two consecutive points at which the curvature becomes zero. Unfortunately in many real cases the loads applied to the structures excite more than one mode and with different amplitudes. Wang et al. ([23]) proposed a new controllability index to find the optimal position of the piezoelectric patches to study modal and multimodal vibrations. They illustrated various beam configurations with a pair of collocated piezoelectric patch

actuators. In Ref. [24], some of the authors of the present contribution have proposed a new function to find the optimal placement of piezoelectric plates to reduce the multimodal vibrations of a fixed cantilever beam. To support their model an experimental apparatus has been built ([25]-[26]). The results have shown a very good agreement between experimental, numerical and theoretical predictions. In this paper, the methodology proposed by Botta et al. ([24]) has been extended to a rotating cantilever beam. The proposed analytical solutions have been also compared with the results of numerical solutions performed using a commercial multi-physics FEM package (COMSOL). Also in this case an experimental apparatus has been designed and constructed and the preliminary results have been reported in Refs. [27], [28].

## II. Governing Equations for Piezoelectric Coupled Blades

In Fig. 1 a schematic of a rotating beam with the attached piezoelectric plates is depicted[1]. In order to control the vertical vibrations an electric field has been applied perpendicular to the two PZT patches. In fact, depending on the sign of the electric field ([29]), they will be deformed in extension or contraction. Applying two out of phase harmonics electric fields to the opposite piezoelectric plates, shear forces will be transferred, via the glue, to the beam. Crawley and de Luis ([4]) have shown that, if the plates are perfectly bonded to the beam, their action can be considered as concentrated at the ends of the plates and it can be modeled by two harmonic flexural moments concentrated at their ends (Fig. [1]).

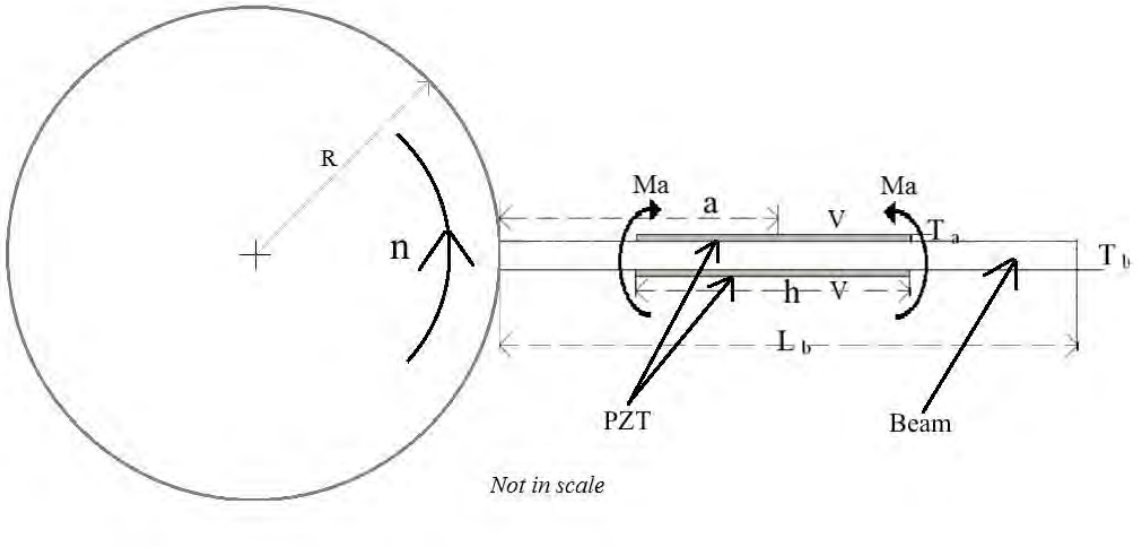


Fig. 1: Reference configuration and action of the PZT plates

The expression of Ma(t) has been derived in ([4]):

$$M_a(t) = \frac{\psi}{6+\psi} E_a c T_a T_b \Lambda(t) \tag{1}$$

with:

$$\begin{cases} \Lambda(t) = \dfrac{d_{31}}{T_a} V(t) \\ \psi = \dfrac{E_b T_b}{E_a T_a} \end{cases} \tag{2}$$

The parameters *a* and *h* characterize the position and the dimensions of the PZT plates (Fig. 1). The aim of this paper is to find their optimal value to damp the multimode vibrations induced on the beam by an external load. To compare different values, the tip of the beam has been chosen as a reference point. In fact all the considered eigenmodes of the rotating cantilever beam have their maximum amplitude at the tip, so that reducing its vibration amplitude the vibration of the entire beam will be reduced as well. If the PZT concentrated moments are in counter phase to the external load, the piezoelectric plates exhibit an active damping effect. The greater is the PZT vibration amplitude induced at the tip, the greater is their ability to damp the vibrations or, in other

[1] In the following the PZT plates will be considered perfectly bonded to the structure, their mass and inertia moment (with respect to the neutral axis of the transverse section of the beam) negligible with respect to the mass and the inertia of the beam and their thickness very lower than the thickness of the beam

words, the greater is their effectiveness. Therefore, the focus of this study is: to find the values of *a* and *h* that maximize the amplitude tip vibration for an assigned a load spectrum, or equivalently, a spectrum provided to the electric field ([4]).

The equilibrium equations are derived by applying the principle of virtual work; considering an Euler-Bernoulli beam and indicating with $\delta L_a$, $\delta L_e$, $\delta L_{in}$, the virtual work of the piezoelectric actuators, elastic and inertial forces, respectively, the principle of the virtual works can be written as :

$$\delta L_a + \delta L_e + \delta L_{in} = 0 \tag{3}$$

Indicating with *w* the vertical displacement, the virtual work of the PZT plates will be[2]:

$$\delta L_a = M_a \left( \left. \frac{\partial \tilde{w}}{\partial x} \right|_{x=a+\frac{h}{2}} - \left. \frac{\partial \tilde{w}}{\partial x} \right|_{x=a-\frac{h}{2}} \right) \tag{4}$$

The variables a and h can vary within the domain identified by the following system equations:

$$\begin{cases} 0 \le a - \dfrac{h}{2} \le L_b \\ 0 \le a + \dfrac{h}{2} \le L_b \\ 0 \le a \le L_b \\ 0 \le h \le L_b \end{cases} \tag{5}$$

Their optimal value strongly depends on the modes that must be damped ([22]).

The virtual work of the elastic and inertial forces can be written, respectively, as ([30]-[32]):

$$\delta L_e = E_b S_b \int_0^{L_b} \left[ \frac{\partial u}{\partial x} + \frac{1}{2}\left(\frac{\partial w}{\partial x}\right)^2 \right] \frac{\partial \tilde{u}}{\partial x} dx + E_b S_b \int_0^{L_b} \left[ \frac{\partial u}{\partial x}\frac{\partial w}{\partial x} + \frac{1}{2}\left(\frac{\partial w}{\partial x}\right)^3 \right] \frac{\partial \tilde{w}}{\partial x} dx + E_b I_b \int_0^{L_b} \frac{\partial^2 w}{\partial x^2}\frac{\partial^2 \tilde{w}}{\partial x^2} dx \tag{6}$$

$$\begin{aligned} \delta L_{in} = {} & \rho_b S_b \int_0^{L_b} \left[ \Omega^2 \left( R + x + u \right) - \ddot{u} + 2\Omega \dot{w} \right] \tilde{u}\, dx + \rho_b S_b \int_0^{L_b} \left[ \Omega^2 w - \ddot{w} - 2\Omega \dot{u} \right] \tilde{w}\, dx \\ & - \rho_b I_b \int_0^{L_b} \left[ \Omega^2 \frac{\partial w}{\partial x} - \frac{\partial \ddot{w}}{\partial x} \right] \frac{\partial \tilde{w}}{\partial x} dx \end{aligned} \tag{7}$$

Integrating by parts the previous equations, we obtain:

$$\begin{aligned} \delta L_e = {} & -E_b S_b \int_0^{L_b} \left[ \frac{\partial^2 u}{\partial x^2} + \frac{\partial w}{\partial x}\frac{\partial^2 w}{\partial x^2} \right] \tilde{u} dx - E_b \int_0^{L_b} \left[ S_b \frac{\partial^2 u}{\partial x^2}\frac{\partial w}{\partial x} + S_b \frac{\partial u}{\partial x}\frac{\partial^2 w}{\partial x^2} + S_b \frac{3}{2}\left(\frac{\partial w}{\partial x}\right)^2 \frac{\partial^2 w}{\partial x^2} - I_b \frac{\partial^4 w}{\partial x^4} \right] \tilde{w} dx + \\ & + E_b S_b \left[ \frac{\partial u}{\partial x} + \frac{1}{2}\left(\frac{\partial w}{\partial x}\right)^2 \right] \tilde{u} \Big|_0^{L_b} + E_b \left[ S_b \frac{\partial u}{\partial x}\frac{\partial w}{\partial x} + \frac{1}{2} S_b \left(\frac{\partial w}{\partial x}\right)^3 - I_b \frac{\partial^3 w}{\partial x^3} \right] \tilde{w} \Big|_0^{L_b} + E_b I_b \frac{\partial^2 w}{\partial x^2}\frac{\partial \tilde{w}}{\partial x} \Big|_0^{L_b}. \end{aligned} \tag{8}$$

[2] The virtual quantities are oversigned by a tilde.

$$\delta L_{in} = \rho_b S_b \int_0^{L_b} \left[ \Omega^2 \left( R + x + u \right) - \ddot{u} + 2\Omega \dot{w} \right] \tilde{u}\, dx + \rho_b \int_0^{L_b} \left[ S_b \Omega^2 w - S_b \ddot{w} - 2 S_b \Omega \dot{u} - \Omega^2 I_b \frac{\partial^2 w}{\partial x^2} + I_b \frac{\partial^2 \ddot{w}}{\partial x^2} \right] \tilde{w}\, dx$$

$$+ \rho_b I_b \left[ \Omega^2 \frac{\partial w}{\partial x} - \frac{\partial \ddot{w}}{\partial x} \right] \tilde{w} \Big|_0^{L_b} \tag{9}$$

Substituting the (4), (8) and (9) into (3), neglecting the terms of higher order and the Coriolis effect, and equating the coefficients of $\tilde{u}$ and $\tilde{w}$ in the integrals, the following equations are obtained:

$$E_b S_b \frac{\partial^2 u}{\partial x^2} = \rho_b S_b \left[ \Omega^2 \left( R + x + u \right) - \ddot{u} \right] \tag{10}$$

$$-E_b \int_0^{L_b} \left[ S_b \frac{\partial^2 u}{\partial x^2} \frac{\partial w}{\partial x} + S_b \frac{\partial u}{\partial x} \frac{\partial^2 w}{\partial x^2} + S_b \frac{3}{2} \left( \frac{\partial w}{\partial x} \right)^2 \frac{\partial^2 w}{\partial x^2} - I_b \frac{\partial^4 w}{\partial x^4} \right] \tilde{w} dx =$$

$$\rho_b \int_0^{L_b} \left[ S_b \Omega^2 w - S_b \ddot{w} - \Omega^2 I_b \frac{\partial^2 w}{\partial x^2} + I_b \frac{\partial^2 \ddot{w}}{\partial x^2} \right] \tilde{w}\, dx + M_a \left( \frac{\partial \tilde{w}}{\partial x} \Big|_{x=a+\frac{h}{2}} - \frac{\partial \tilde{w}}{\partial x} \Big|_{x=a-\frac{h}{2}} \right) \tag{11}$$

with these boundary conditions for *u*:

$$\begin{cases} u(0) = 0 \\ u^I \left( L_b \right) = 0 \end{cases} \tag{12}$$

and for *w*:

$$\begin{cases} w(0) = 0 \\ w^I \left( 0 \right) = 0 \\ w^{II} \left( L_b \right) = 0 \\ w^{III} \left( L_b \right) = 0 \end{cases} \tag{13}$$

Neglecting the axial accelerations $\ddot{u}$, which are small compared to the centripetal acceleration $\Omega^2(R+x+u)$, the solution of the system (10), (12) yields:

$$u(x) = \frac{\Omega^2 \rho_b}{E_b} \left( -\frac{x^3}{6} - \frac{R x^2}{2} + R L_b x + \frac{L_b^2 x}{2} \right) \tag{14}$$

Taking into account equation (14), *w* is the only unknown quantity in (11). Moreover using the modal analysis technique, and indicating with $\phi_i(x)$ the *i-th* flexural modal displacement of the rotating cantilever beam and with $X_i(t)$ its amplitude, the vertical displacement can be approximated by:

$$w(x,t) = \sum_{i=1}^{N} X_i(t) \phi_i(x) \tag{15}$$

so that substituting equations (14) and (15) in equation (11) the following vectorial governing equation is obtained:

$$\mathbf{M} \ddot{\mathbf{X}}(t) + \mathbf{K} \mathbf{X}(t) = \mathbf{B}(a,h) V(t) \tag{16}$$

where **X** represents the vector of the amplitudes of the modes, **M** and **K** are the mass and the stiffness matrices and are given by:

$$\begin{cases} \mathbf{M} = \mathbf{M}_1 - \mathbf{M}_2 \\ \\ \mathbf{K} = \mathbf{K}_1 - \mathbf{K}_2 - \mathbf{K}_3 - \Omega^2 \left( \mathbf{M}_1 - \mathbf{M}_2 \right) \end{cases} \tag{17}$$

and **B**(a; h) is the vector control:

$$B\left(a,h\right) = \tilde{M}\left[ \phi_1^I\left(a+\frac{h}{2}\right) - \phi_1^I\left(a-\frac{h}{2}\right), \phi_2^I\left(a+\frac{h}{2}\right) - \phi_2^I\left(a-\frac{h}{2}\right), ..., \phi_N^I\left(a+\frac{h}{2}\right) - \phi_N^I\left(a-\frac{h}{2}\right) \right] \tag{18}$$

with $\tilde{M} = \left(\frac{\psi}{6+\psi}\right) E_a c T_a T_b \frac{d_{31}}{T_a}$. If the Rayleigh damping is considered, the equation (16) develops into:

$$\mathbf{M}\ddot{\mathbf{X}}(t) + \mathbf{C}\dot{\mathbf{X}}(t) + \mathbf{K}\mathbf{X}(t) = \mathbf{B}\left(a,h\right)V(t) \tag{19}$$

with:

$$\mathbf{C} = \alpha\mathbf{M} + \beta\mathbf{K} \tag{20}$$

Considering the normal modes the mass and stiffness matrices become: **M** = **I**, **K** = $\boldsymbol{\omega}^2$ where **ω** is the diagonal matrix of the eigenvalues of the beam and **I** the identity matrix. Assuming β = 0, equation (19) is simplified in the following form:

$$\ddot{\mathbf{X}}(t) + \alpha\dot{\mathbf{X}}(t) + \boldsymbol{\omega}^2\mathbf{X}(t) = \mathbf{B}V(t) \tag{21}$$

The optimal placement for a single mode has been found by Barboni et al ([22]). Neverthless if the load spectrum includes various modes, with different amplitudes, e.g. gas turbine blades, to the author knowledge an analytical method has not yet been established. Here a new function is proposed, and the analytical results are compared with the numerical obtained using a multi-physics FEM package. Therefore, recalling that assigning a spectrum to the external load is equivalent, from the point of view of the aim of this paper, to assign a spectrum to the PZT applied voltage, and indicating with $N_s$ the number of the excited modes:

$$V(t) = \sum_{j=1}^{Ns} V_j \cos(\omega_j t) \tag{22}$$

The solution of equation (21) becomes:

$$X_i\left(t\right) = \sum_{j=1}^{N_s} - \frac{e^{-\frac{t\alpha}{2}} B_i V_j \cosh\left(\frac{1}{2}t\sqrt{\alpha^2 - 4\omega_i^2}\right)\sqrt{\alpha^2 - 4\omega_i^2}\left(\omega_i^2 - \omega_j^2\right)}{\sqrt{\alpha^2 - 4\omega_i^2}\left[\alpha^2\omega_j^2 + \left(\omega_i^2 - \omega_j^2\right)^2\right]} +$$

$$- \frac{e^{-\frac{t\alpha}{2}} B_i V_j \alpha \sinh\left(\frac{1}{2}t\sqrt{\alpha^2 - 4\omega_i^2}\right)\left(\omega_i^2 + \omega_j^2\right)}{\sqrt{\alpha^2 - 4\omega_i^2}\left[\alpha^2\omega_j^2 + \left(\omega_i^2 - \omega_j^2\right)^2\right]} + \frac{B_i V_j \alpha \sin\left(\omega_j t\right)\omega_j}{\alpha^2\omega_j^2 + \left(\omega_i^2 - \omega_j^2\right)^2} + \frac{B_i V_j \cos\left(\omega_j t\right)\left(\omega_i^2 - \omega_j^2\right)}{\alpha^2\omega_j^2 + \left(\omega_i^2 - \omega_j^2\right)^2} \tag{23}$$

An approximation form of (23) has been obtained considering that the contribution of the i-th term is predominant:

$$X_i(a,h,t) \cong \frac{B_i V_i sin(\omega_i t)}{\alpha\omega_i} - \frac{e^{-\frac{1}{2}t(\alpha+\sqrt{\alpha^2-4\omega_i^2})}\left(-1+e^{t(\alpha+\sqrt{\alpha^2-4\omega_i^2})}\right)B_i V_i}{\alpha\sqrt{\alpha^2-4\omega_i^2}} \tag{24}$$

The second term of the right hand side of equation (24) represents the transient part so that if this is neglected, the amplitude of the displacement of the free end of the beam can be written as:

$$| w(a,h,L_b) | = \sum_{i=1}^{N_s} \left| \frac{B_i(a,h) V_i \phi_i(L_b)}{\alpha\omega_i} \right| \tag{25}$$

In the following, in order to simplify the discussion of the results obtained by the general formulation, a bimodal excitation is taken into account. The numbers $i_1$, $i_2$ indicate the indexes of the first and the second considered mode respectively, $r$ ($\leq 1$) is a coefficient determining the contribution to the excitation induced by the second considered mode with respect to the first: $r = 1$ corresponds to the second mode governing the excitation without any contribution from the first.

Therefore from equation (22):

$$V(t) = (1-r)cos(\omega_{i_1} t) + rcos(\omega_{i_2} t) \tag{26}$$

Substituting equation (26) into equation (25) and introducing the function:

$$\begin{cases} g_{i_1}(r,\xi) = \dfrac{\tilde{M}}{\alpha}\dfrac{1-r}{\omega_{i_1}}\phi_{i_1}(L_b)\phi_{i_1}^I(\xi) \\ \\ g_{i_2}(r,\xi) = \dfrac{\tilde{M}}{\alpha}\dfrac{r}{\omega_{i_2}}\phi_{i_2}(L_b)\phi_{i_2}^I(\xi) \end{cases} \tag{27}$$

we obtain:

$$\left|\widehat{w}(r,a,h)\right| = \left| g_{i_1}\left(r, a+\frac{h}{2}\right) - g_{i_1}\left(r, a-\frac{h}{2}\right)\right| + \left| g_{i_2}\left(r, a+\frac{h}{2}\right) - g_{i_2}\left(r, a-\frac{h}{2}\right)\right| \tag{28}$$

Indicating with $\xi_1 = a + h/2$ and $\xi_2 = a - h/2$, respectively, the position of the right and left ends of the piezo plates, equation (28) gives:

$$\left|\widehat{w}(r,\xi_1,\xi_2)\right| = \left| g_{i_1}(r,\xi_1) - g_{i_1}(r,\xi_2)\right| + \left| g_{i_2}(r,\xi_1) - g_{i_2}(r,\xi_2)\right| \tag{29}$$

Assigned the coefficient $r$, and denoting with $(\hat{\xi}_1, \hat{\xi}_2)$ the coordinates of the absolute maximum of $\left|\widehat{w}(r,\xi_1,\xi_2)\right|$ it is possible to write:

$$\left|\widehat{w}(r,\xi_1,\xi_2)\right|_{max} = \left|\widehat{w}(r,\hat{\xi}_1,\hat{\xi}_2)\right| = \left| g_{i_1}(r,\hat{\xi}_1) - g_{i_1}(r,\hat{\xi}_2)\right| + \left| g_{i_2}(r,\hat{\xi}_1) - g_{i_2}(r,\hat{\xi}_2)\right| \tag{30}$$

Considering that $g_k(r,\xi)$ has, for all the considered values of $k$ and $r$, its positive absolute maximum at $\hat{\xi}_1 = L_b$, this value will be also correspond to the abscissa of the positive absolute maximum for $\left| g_{i_1}(r,\xi_1) - g_{i_1}(r,\xi_2)\right| + \left| g_{i_2}(r,\xi_1) - g_{i_2}(r,\xi_2)\right|$.

This implies that the PZT plates should always be placed with their right edges at the tip of the beam independently of the excited modes, load spectrum and the angular velocity, hence:

$$\left|\widehat{w}(r,\xi_1,\xi_2)\right|_{max} = \left|\widehat{w}(r,L_b,\hat{\xi}_2)\right|_{max} = \left| g_{i_1}(r,L_b) - g_{i_1}(r,\hat{\xi}_2)\right| + \left| g_{i_2}(r,L_b) - g_{i_2}(r,\hat{\xi}_2)\right| \tag{31}$$

Moreover since:

$$0 < g_j\left(r, L_b\right) > g_j\left(r, \xi\right) \quad \forall \xi \in [0, L_b); \quad \forall j \tag{32}$$

equation (31) becomes:

$$\left|\hat{w}\left(r, \xi_1, \xi_2\right)\right|_{max} = \left|\hat{w}\left(r, L_b, \hat{\xi}_2\right)\right|_{max} = f_{i_1}\left(r, L_b\right) - f_{i_2}\left(r, \hat{\xi}_2\right) \tag{33}$$

where:

$$f_{i_1 i_2}\left(r, \xi_2\right) = g_{i_1}\left(r, \xi_2\right) + g_{i_2}\left(r, \xi_2\right) = \frac{\tilde{M}}{\alpha}\left[\left(1-r\right)\frac{\phi_{i_1}\left(L_b\right)}{\omega_{i_1}}\phi_{i_1}^{I}\left(\xi_2\right) + r\frac{\phi_{i_2}\left(L_b\right)}{\omega_{i_2}}\phi_{i_2}^{I}\left(\xi_2\right)\right] \tag{34}$$

Analyzing equation (33) it can be observed that the coordinates $\left(\hat{\xi}_1, \hat{\xi}_2\right)$ of the absolute maximum of $\left|\hat{w}\left(r, \xi_1, \xi_2\right)\right|$ will coincide, respectively, with the abscissa of the absolute maximum, $\hat{\xi}_1 = L_b$ and minimum of the function $f_{i_1 i_2}\left(r, \xi_2\right)$. The position of the absolute minimum depends on the considered coupled modes $i_1$, $i_2$ , the angular velocity $n$ (because it influences the shape of the modes $\phi_{i_2}\left(\xi_2\right)$) and the modes ratio $r$; thus the optimal location of the left edges of the PZT elements can be found by solving the following system of equations:

$$\begin{cases} \dfrac{\partial f_{i_1 i_2}\left(r, \xi_2\right)}{\partial \xi_2} = \dfrac{\tilde{M}}{\alpha}\left[\left(1-r\right)\dfrac{\phi_{i_1}\left(L_b\right)}{\omega_{i_1}}\phi_{i_1}^{II}\left(\xi_2\right) + r\dfrac{\phi_{i_2}\left(L_b\right)}{\omega_{i_2}}\phi_{i_2}^{II}\left(\xi_2\right)\right] = 0 \\ \dfrac{\partial^2 f_{i_1 i_2}\left(r, \xi_2\right)}{\partial \xi_2{}^2} = \dfrac{\tilde{M}}{\alpha}\left[\left(1-r\right)\dfrac{\phi_{i_1}\left(L_b\right)}{\omega_{i_1}}\phi_{i_1}^{III}\left(\xi_2\right) + r\dfrac{\phi_{i_2}\left(L_b\right)}{\omega_{i_2}}\phi_{i_2}^{III}\left(\xi_2\right)\right] > 0 \end{cases} \tag{35}$$

The solution will provide all the local minima and the absolute minimum will then be selected among these. It is worth noting that for *r=0*, or *r=1*, $f_{i_1 i_2}$ is proportional to the first spatial derivative of the first, or the second, considered mode respectively; hence, in these cases its absolute minimum will correspond to that of the individual derivative modes considered in isolation.

## III. Results and Discussion

In this section the results of the proposed analytical model, and their comparison with those obtained by the performed FEM simulations, are reported. For the FEM simulations the Prestressed Analysis, Frequency Domain Study of the Structural Mechanics Module of COMSOL Multiphysics software has been used. The model considers a steel beam of *30 cm* of length, *3 cm* of width and *3 mm* of thickness. The radius of the hub, *R*, has been chosen to be *1 m*.

In order to consider different bimodal excitations, and focusing on the first five modes, the wavelength of the fifth mode has been approximately divided in 50 subintervals of 3 *mm* in length, so that $\Delta a = \Delta h = 3$ *mm*. Consequently 5000 different points of the $\{a,h\}$ domain have been considered, each of these characterize the position of the applied harmonic PZT moment (Fig. 1). The frequencies of these applied moments have been chosen to correspond to the first five eigenfrequencies of the beam. For each of these frequencies the vibration amplitude of the tip of the beam has been calculated, while the amplitude to a their linear combination has been obtained by superposition of the previous responses. For every combination, the optimal position of the PZT elements has been chosen to be the one which corresponds to the maximum tip vibration amplitude. This procedure has been repeated for every considered angular velocity. Before analysing the results, it must be observed that the function $f_{i_1 i_2}$ is the sum of two terms: the first relative to mode $i_1$ and the second relative to mode $i_2$ (see equation (34)). For low values of $r$ the first prevails; as $r$ increases the contribution of the second considered mode, $i_2$, increases until it becomes dominant. Therefore, it is expected that the absolute minimum of $f_{i_1 i_2}$ varies from the absolute minimum obtained for mode $i_1$ to the absolute minimum of mode $i_2$ following a path that depends on the considered modes. Vice versa, as demonstrated above and also discussed in [24], there is no question about the position of the absolute maximum: this is always at the tip of the beam. In our model the computed absolute

minimum and maximum correspond, respectively, to the optimal placement of the left and right terminations of the PZT plates to be chosen in order to obtain the optimal damping of the considered bimodal combinations.

The first example results relate to the study of the coupling between the first and the second mode; Fig. 2 plot the function $f_{1,2}$, for different values of *r* and *n*. The results for the optimal positions are summarized in Fig. 3. The red curve represents the positions of the absolute maximum (see Fig. 3 (b)) and, as expected, they are invariably at $\overline{\xi}_2 = 1$; however the positions of the absolute minimum depend on *r* and *n* (see Fig. 3 (a)). For *r=0* the two computed locations corresponds to the optimal placement to be used to damp the first mode (see eq. (26) and [22]-[24]). The change of the shape of the first mode with *n* does not affect the positions of the extreme values of its first derivative ([33]): this suggests that using piezoelectric plates that cover the entire beam, will invariably be the optimal solution if the aim is to damp the first mode of vibration. Otherwise the influence of the angular velocity of the shaft on the position of the absolute minimum of the first derivative of the second mode (see [33] and Fig. 4), implies a change of the optimal configuration, to damp the second mode, with *n* (*r =1* in Fig. 3 (a)). Moreover, the results reported in Fig. 3 (a) also show that for values of *r* less than $\hat{r}$ the optimal configuration corresponds to that obtained for the first mode considered in isolation, and only for $r > \hat{r}$ starts to change. This *"take-off"* value $\hat{r}$ depends on the angular velocity *n* and it can be explained by observing that for $0 \le r < \hat{r}$ $f_{1,2}$ has a minimum at the boundary point $\overline{\xi}_2 = 0$, but this is not a stationary point (see Fig. 2 (a)-(b)). Increasing *r* the shape of $f_{1,2}$ changes and only when *r* becomes equal to $\hat{r}$, $\overline{\xi}_2 = 0$ becomes a stationary point. For r> $\hat{r}$ the absolute minimum point of $f_{1,2}$ remains a stationary point, and the optimal position of the left side of the PZT plates begins to move to reach, at *r=1*, the optimal configuration which would be obtained considering the second mode in isolation (Fig. 3 (a)). To emphasize this phenomenon, two zoomed plot, for *r=0.6* and *r=0.8* focusing on the region where $f_{1,2}$ experiences a minimum, have been reported in Fig. 5. Therefore, $\hat{r}$ can be obtained by search the value of *r* where the first derivative of $f_{1,2}$, with respect to $\xi_2$, is zero for $\overline{\xi}_2 = 0$; thus, from the equation (35.1):

$$\hat{r} = \frac{\phi_1^{II}(0)\phi_1(1)}{\phi_1^{II}(0)\phi_1(1) - \phi_2^{II}(0)\phi_2(1)\dfrac{\omega_1}{\omega_2}} \tag{36}$$

To study the coupling between *2nd-3rd* and *3rd-4th* modes the functions $f_{2,3}$, $f_{3,4}$ are pictured in Figs. 7, 10. In these cases there is a constant gradual transition from the first to the second optimal configuration (Fig. 8 and Fig. 11). It can be noticed that, also in these cases, when *n* increases, the shapes of the first derivative of the third and fourth mode changes (see Fig. 6 and 9), and the optimal configuration to damp these modes is, therefore, modified. The optimal positions of the right side for the coupling between the third and the fourth mode have not been reported because the results are very similar to those shown in Fig. 3 and in Fig. 8.

Observing Fig. 12 it can be noticed that, differently from the others considered modes, there is an abrupt transition of the absolute minimum of $\phi_5^I(\overline{\xi}_2)$ with *n*; this is, approximately, at $\overline{\xi}_2 = 0.25$ until *n=2000 rpm* and then it shifts to $\overline{\xi}_2 = 0.75$ (see Fig. 12 (b)). This could entails abrupt transition of the PZT optimal position when the fifth mode is one of the coupled modes. For example in Fig. 13 and in Fig. 14 are reported the results when the fifth mode is coupled to the second. The behaviour for *n=0 rpm, 1000 rpm, 2000 rpm* is rather regular, but a sharp transition is experienced, near *r=1*, for the other velocities (see for example plots for *n=3000 rpm, 4000 rpm, 5000 rpm* in Fig. 14). This can be explained analysing Fig. 15. For *r=0* $f_{2,5}$ is proportional to $\phi_2^I(\overline{\xi}_2)$ and there is only one minimum and one maximum. The same trend is found when the contribution of the fifth mode increases until *r* reaches a value, *r≈0.46* for *n=1000 rpm* and , *r≈0.36* for *n=5000 rpm*, where another minimum (and a maximum) appears near $\overline{\xi}_2 = 0.6$. The reason of the transition is that for *n = 5000 rpm* (for example), next to *r=1* , this develops into an absolute minimum at $\overline{\xi}_2 = 0.7$. An analogous behavior is obtained for *n = 3000 rpm and 4000 rpm*.

When the fifth mode is coupled with the third mode (see Fig. 16 and Fig. 17) a different behaviour is obtained when varying the rotational speed. The optimal placement of the left-hand side of the PZT plates is almost independent of *n* for low values of *r* but a bifurcation is observed for values around *r=0.3*, whereby for *n < 2000 rpm* the optimal location points to the left and above *n = 2000 rpm* the optimal locations move towards the right.

The velocity *n=2000 rpm* is between the two fields, there is initially a trend to right then a sharp transition to the left. This behaviour correspond to the location of the absolute minimum of $\phi_5^I\left(\overline{\xi}_2\right)$ (Fig. 12).

Also in these cases the results for the optimal positions of the right side of the PZT actuators are analogous to those shown in Fig. 3 and in Fig. 8.

All comparisons performed between the FEM simulations and the proposed model, to corroborate the analytical results, have shown a very good agreement between numerical predictions and the solutions. For clarity only the results for three values of *n* (*n = 0, 1000 and 5000 rpm*) are shown.

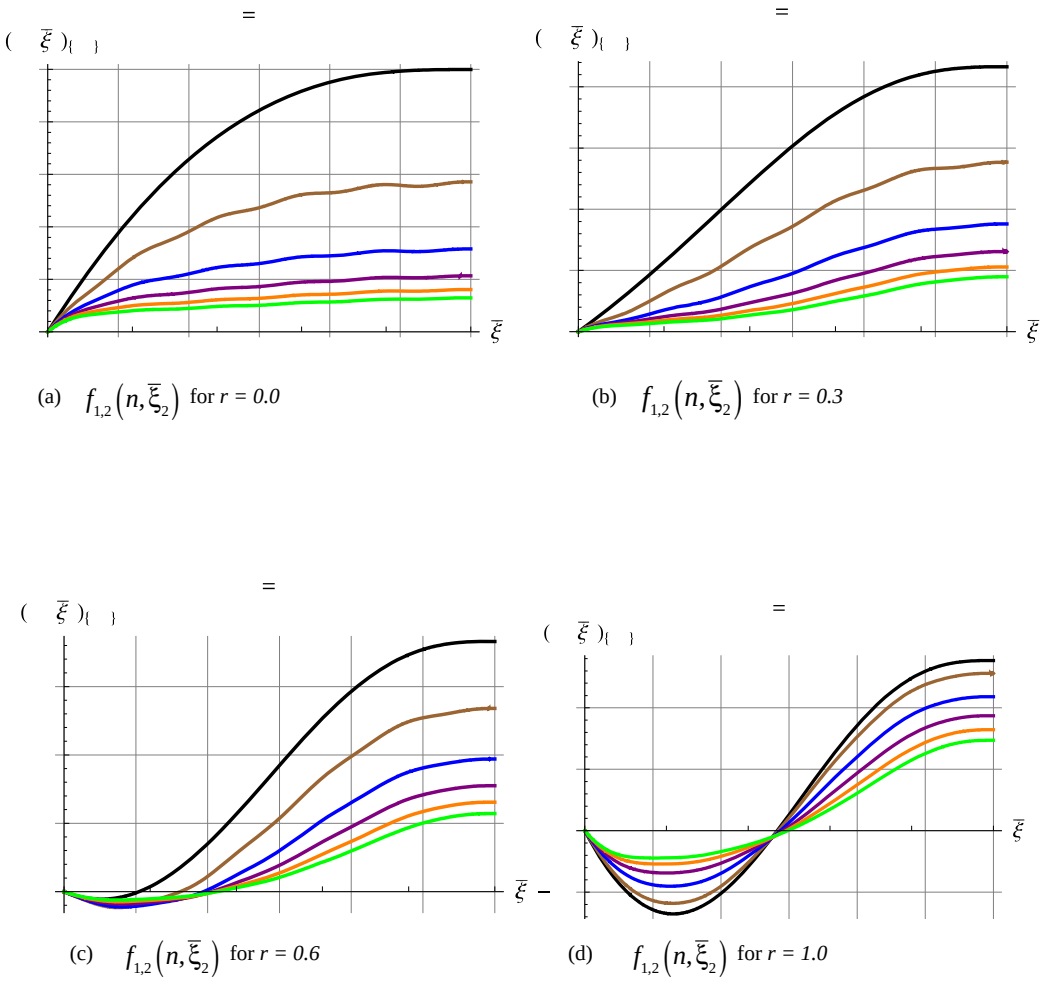

(a) $f_{1,2}\left(n,\overline{\xi}_2\right)$ for *r = 0.0* (b) $f_{1,2}\left(n,\overline{\xi}_2\right)$ for *r = 0.3*

(c) $f_{1,2}\left(n,\overline{\xi}_2\right)$ for *r = 0.6* (d) $f_{1,2}\left(n,\overline{\xi}_2\right)$ for *r = 1.0*

Fig. 2 $f_{1,2}\left(n,\overline{\xi}_2\right)$ *n=0 rpm; n=1000 rpm; n=2000 rpm n=3000 rpm n=4000 rpm n=5000 rpm.*

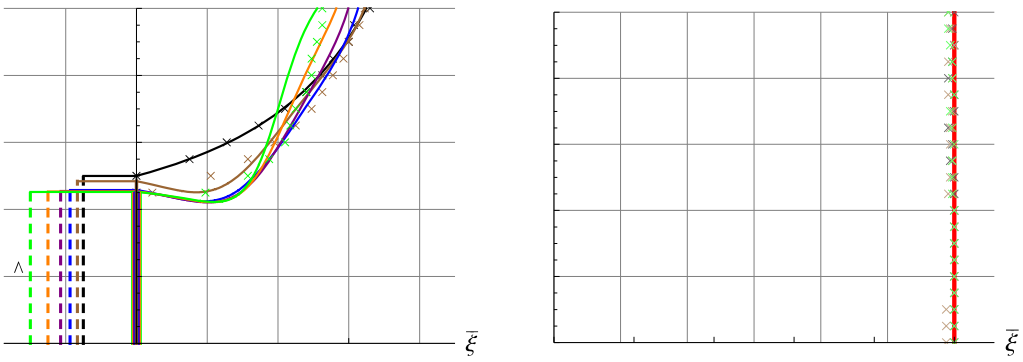

(a) Optimal Placements of the Left Sides (OPLS) (b) Optimal Placements of the Right Sides (OPRS)

Figure 3: Optimal Placements of the Left Sides (OPLS) and Right Sides (OPRS) for the coupling between the first and the second mode by applying the Proposed Analytical Model (PAM) and the Finite Elements Method (FEM). *n=0 rpm* (OPLS-PAM); *n=1000 rpm* (OPLS-PAM); *n=2000 rpm* (OPLS-PAM) *n=3000 rpm* (OPLS-PAM) *n=4000 rpm* (OPLS-PAM) *n=5000 rpm* (OPLS-PAM); all the velocities (OPRS-PAM) × *n=0 rpm* (OPLS-FEM) × *n=1000 rpm* (OPLS-FEM) × *n=5000 rpm* (OPLS-FEM);

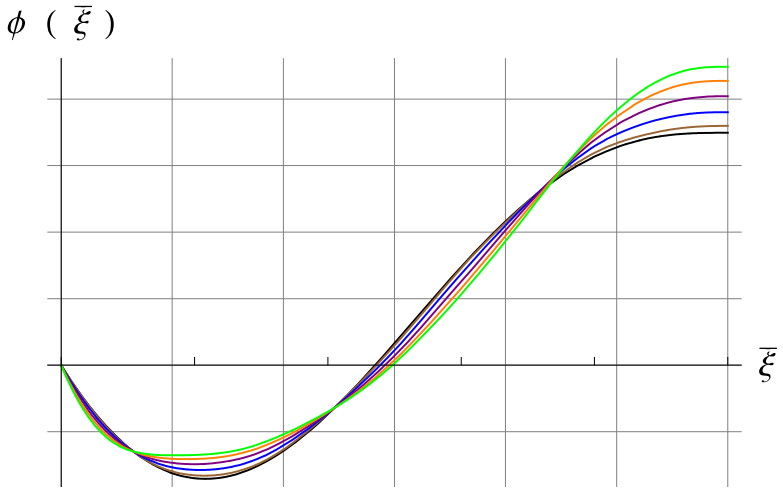

Fig. 4 First derivative of the second mode *n=0 rpm; n=1000 rpm; n=2000 rpm n=3000 rpm n=4000 rpm n=5000 rpm*

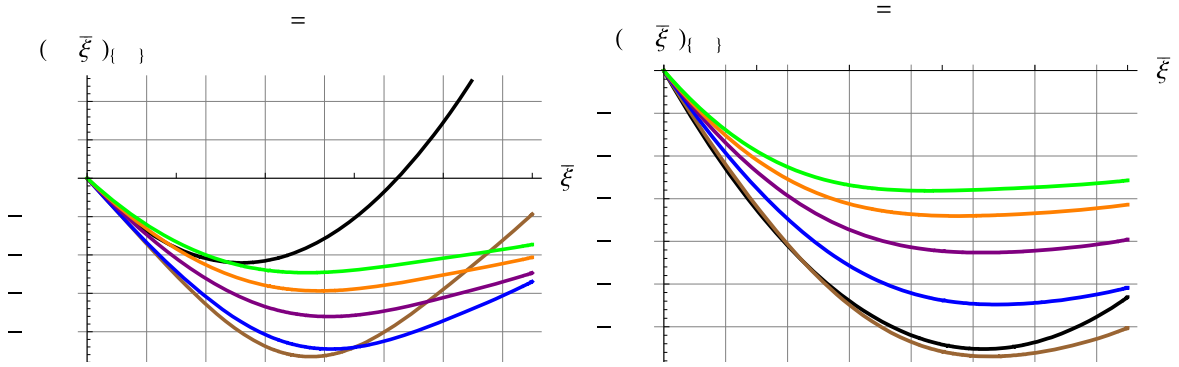

(a) $f_{1,2}\left(n,\overline{\xi}_2\right)$ for $r = 0.6$ (b) $f_{1,2}\left(n,\overline{\xi}_2\right)$ for $r = 0.8$

Fig. 5 Zoom-in of the absolute minimum region of $f_{1,2}\left(n,\overline{\xi}_2\right)$ *n=0 rpm; n=1000 rpm; n=2000 rpm n=3000 rpm n=4000 rpm n=5000 rpm.*

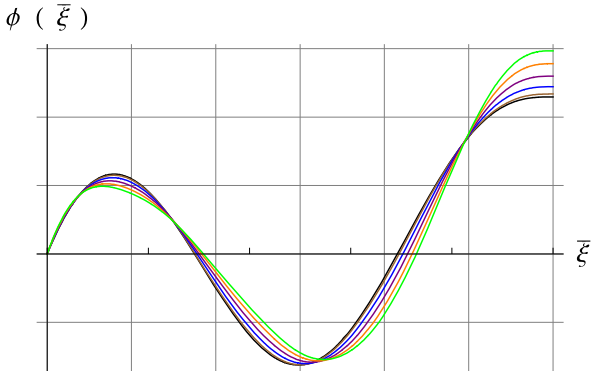

Fig. 6 First derivative of the third mode *n=0 rpm; n=1000 rpm; n=2000 rpm n=3000 rpm n=4000 rpm n=5000 rpm*

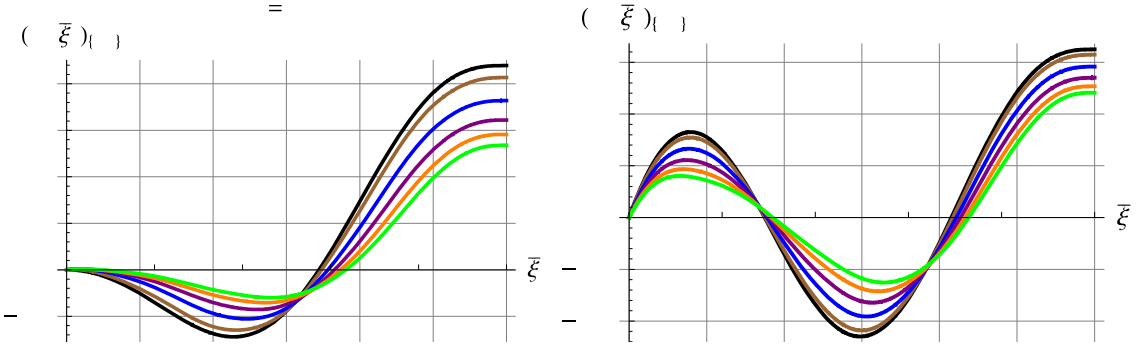

(a) $f_{2,3}\left(n,\overline{\xi}_2\right)$ for $r = 0.5$ (b) $f_{2,3}\left(n,\overline{\xi}_2\right)$ for $r = 1.0$

Fig. 7 $f_{2,3}\left(n,\overline{\xi}_2\right)$ *n=0 rpm; n=1000 rpm; n=2000 rpm n=3000 rpm n=4000 rpm n=5000 rpm.*

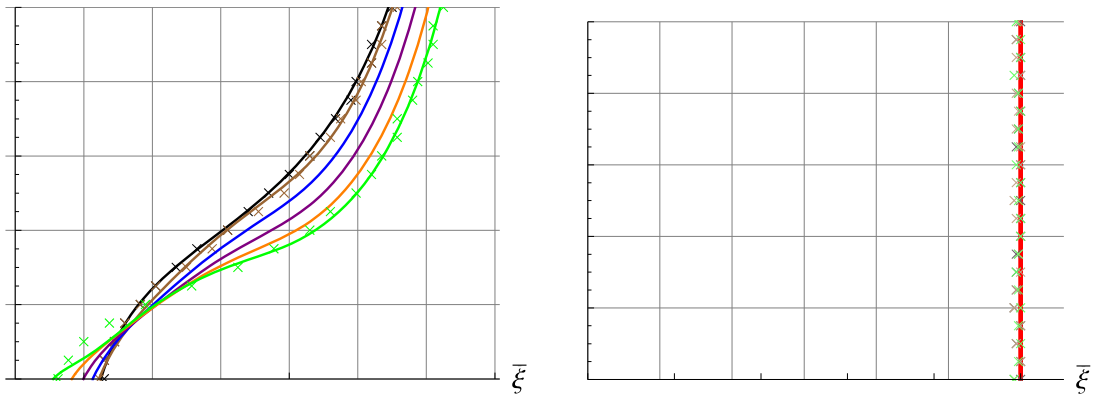

(a) Optimal Placements of the Left Sides (OPLS) (b) Optimal Placements of the Right Sides (OPRS)

Figure 8: Optimal Placements of the Left Sides (OPLS) and Right Sides (OPRS) for the coupling between the second and the third mode by applying the Proposed Analytical Model (PAM) and the Finite Elements Method (FEM). *n=0 rpm* (OPLS-PAM); *n=1000 rpm* (OPLS-PAM); *n=2000 rpm* (OPLS-PAM) *n=3000 rpm* (OPLS-PAM) *n=4000 rpm* (OPLS-PAM) *n=5000 rpm* (OPLS-PAM); all the velocities (OPRS-PAM) × *n=0 rpm* (OPLS-FEM) × *n=1000 rpm* (OPLS-FEM) × *n=5000 rpm* (OPLS-FEM);

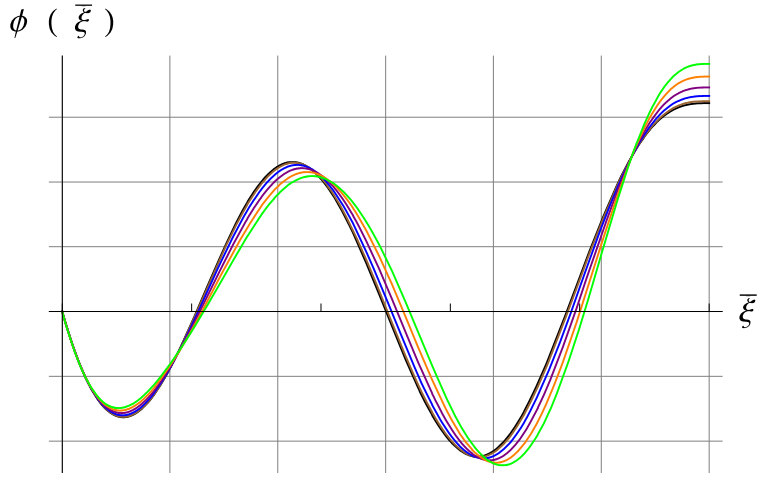

Fig. 9 First derivative of the fourth mode *n=0 rpm; n=1000 rpm; n=2000 rpm n=3000 rpm n=4000 rpm n=5000 rpm*

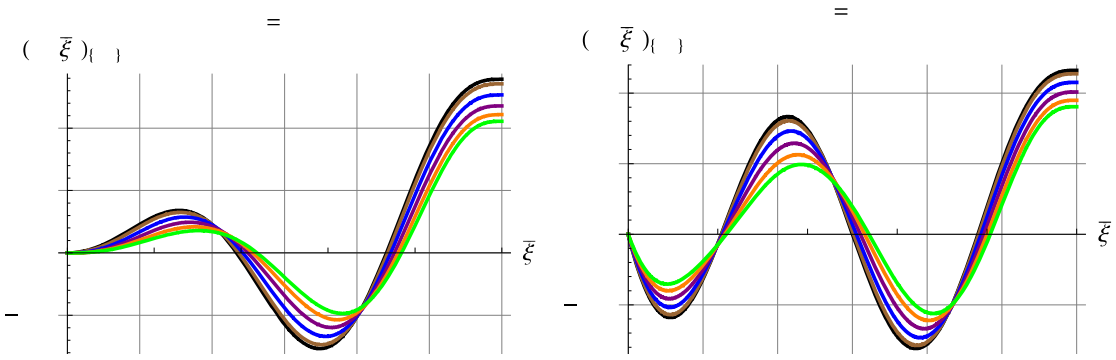

Fig. 10 $f_{3,4}\left(n,\overline{\xi}_2\right)$ *n=0 rpm; n=1000 rpm; n=2000 rpm n=3000 rpm n=4000 rpm n=5000 rpm.*

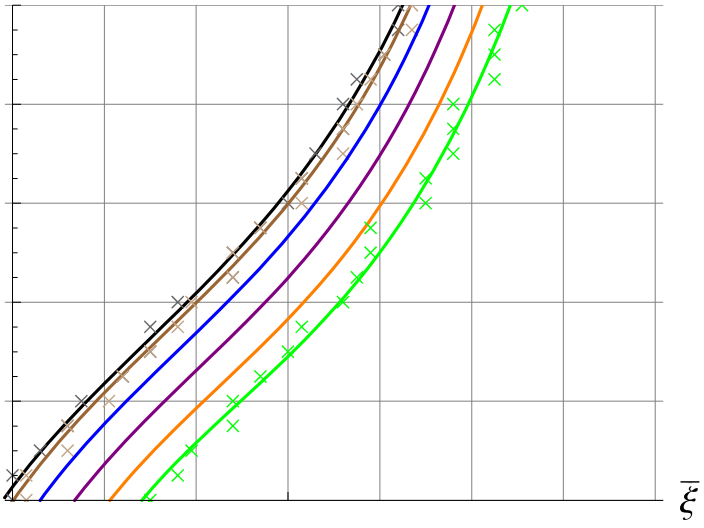

Figure 11: Optimal Placements of the Left Sides (OPLS) for the coupling between the third and the fourth mode by applying the Proposed Analytical Model (PAM) and the Finite Elements Method (FEM). *n=0 rpm* (OPLS-PAM); *n=1000 rpm* (OPLS-PAM); *n=2000 rpm* (OPLS-PAM) *n=3000 rpm* (OPLS-PAM) *n=4000 rpm* (OPLS-PAM) *n=5000 rpm* (OPLS-PAM); all the velocities (OPRS-PAM) × *n=0 rpm* (OPLS-FEM) × *n=1000 rpm* (OPLS-FEM) × *n=5000 rpm* (OPLS-FEM);

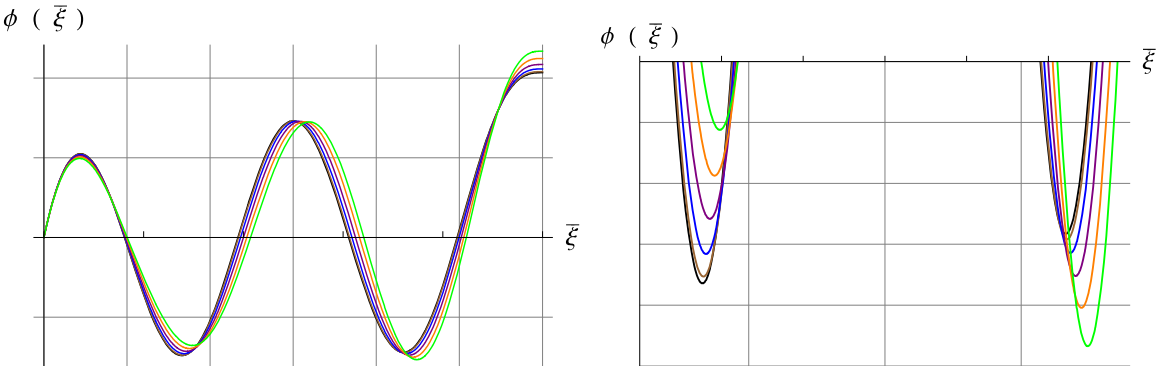

(a) First derivative of the fifth mode

(b) Zoom-in of the minimum region of the first derivative of the fifth mode

Fig. 12 First derivative of the fifh mode *n=0 rpm; n=1000 rpm; n=2000 rpm n=3000 rpm n=4000 rpm n=5000 rpm*

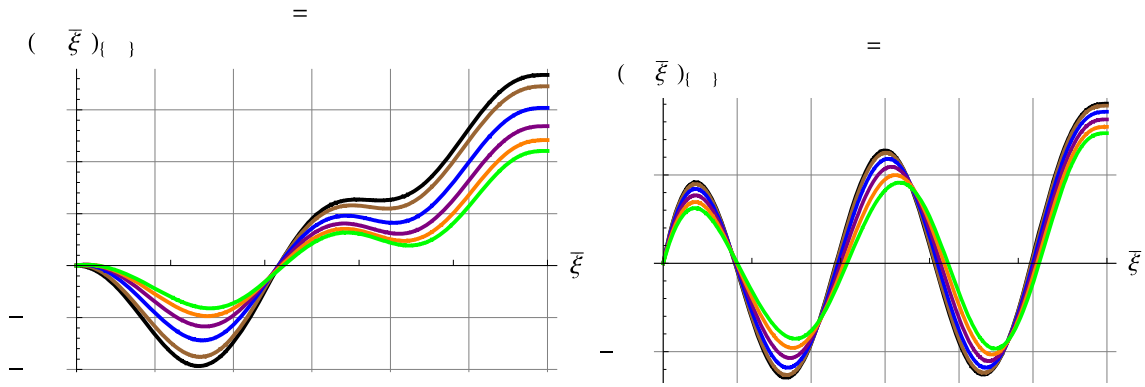

(a) $f_{2,5}\left(n,\overline{\xi}_2\right)$ for $r = 0.5$

(b) $f_{2,5}\left(n,\overline{\xi}_2\right)$ for $r = 1.0$

Fig. 13 $f_{2,5}\left(n,\overline{\xi}_2\right)$ *n=0 rpm; n=1000 rpm; n=2000 rpm n=3000 rpm n=4000 rpm n=5000 rpm.*

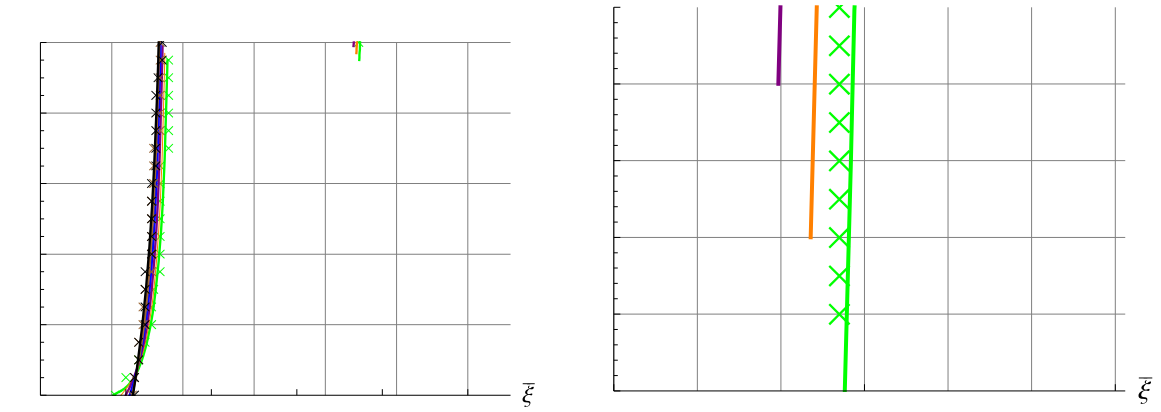

(a) Optimal Placements of the Left Sides (OPLS)

(b) Zoom-in of Optimal Placements of the Left Sides next to *r=1*

Figure 14: Optimal Placements of the Left Sides (OPLS) for the coupling between the second and the fifth mode by applying the Proposed Analytical Model (PAM) and the Finite Elements Method (FEM). *n=0 rpm* (OPLS-PAM); *n=1000 rpm* (OPLS-PAM); *n=2000 rpm* (OPLS-PAM) *n=3000 rpm* (OPLS-PAM) *n=4000 rpm* (OPLS-PAM) *n=5000 rpm* (OPLS-PAM); all the velocities (OPRS-PAM) × *n=0 rpm* (OPLS-FEM) × *n=1000 rpm* (OPLS-FEM) × *n=5000 rpm* (OPLS-FEM);

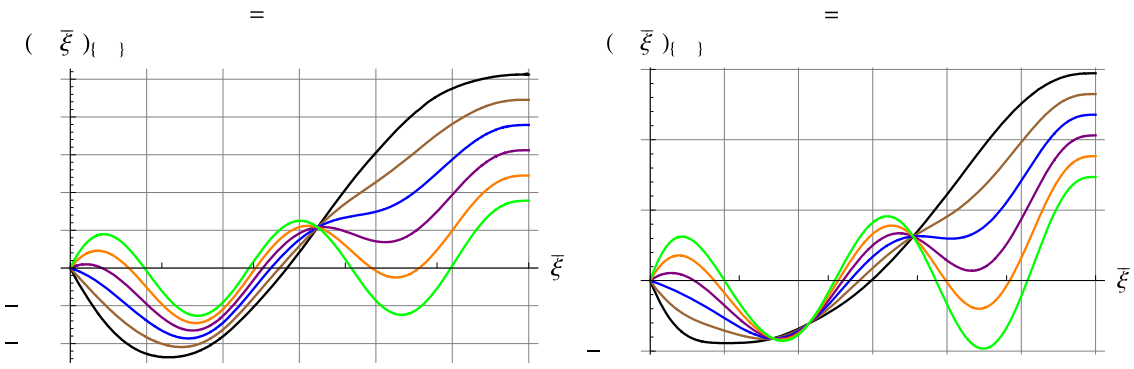

(a) $f_{2,5}\left(r,\bar{\xi}_2\right)$ for $n$ =1000 rpm (b) $f_{2,5}\left(r,\bar{\xi}_2\right)$ for $n$ = 5000 rpm

Fig. 15 $f_{2,5}\left(r,\bar{\xi}_2\right)$ r=0; r=0.2; r=0.4 r=0.6 r=0.8 r=1.0

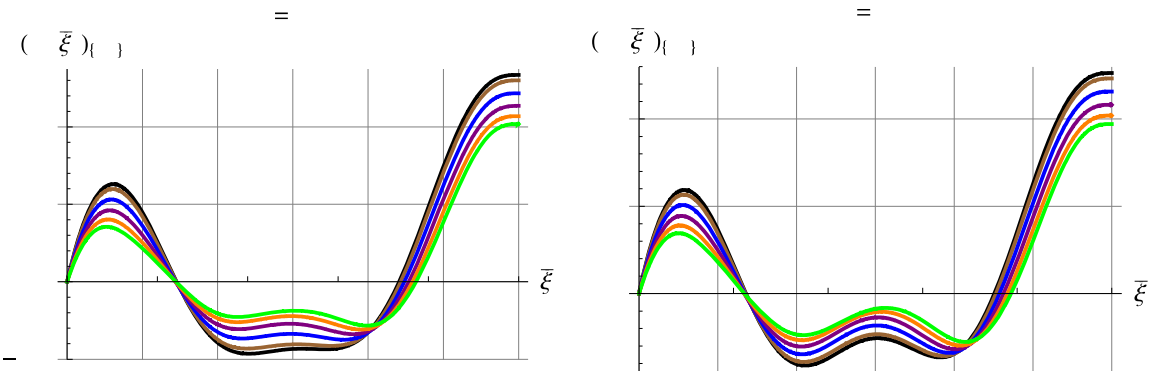

(a) $f_{3,5}\left(n,\bar{\xi}_2\right)$ for $r$ = 0.4 (b) $f_{3,5}\left(n,\bar{\xi}_2\right)$ for $r$ = 0.5

Fig. 16 $f_{3,5}\left(n,\bar{\xi}_2\right)$ n=0 rpm; n=1000 rpm; n=2000 rpm n=3000 rpm n=4000 rpm n=5000 rpm.

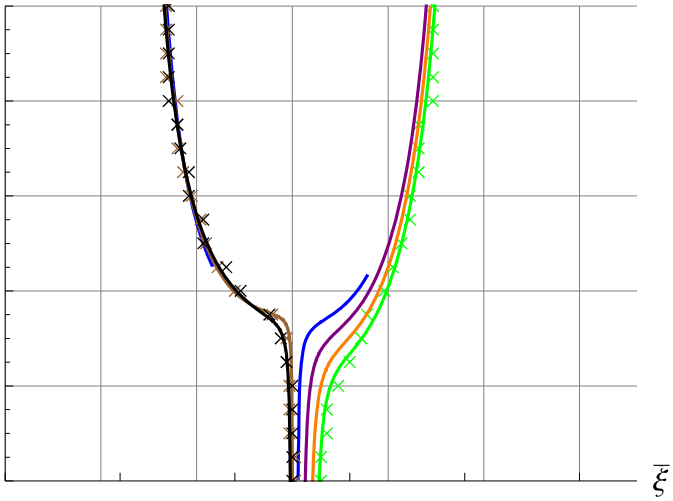

Figure 17: Optimal Placements of the Left Sides (OPLS) for the coupling between the third and the fifth mode by applying the Proposed Analytical Model (PAM) and the Finite Elements Method (FEM). n=0 rpm (OPLS-PAM); n=1000 rpm (OPLS-PAM); n=2000 rpm (OPLS-PAM) n=3000 rpm (OPLS-PAM) n=4000 rpm (OPLS-PAM) n=5000 rpm (OPLS-PAM); all the velocities (OPRS-PAM) × n=0 rpm (OPLS-FEM) × n=1000 rpm (OPLS-FEM) × n=5000 rpm (OPLS-FEM);

## IV. CONCLUSIONS

In [24] some of the authors have proposed a new theoretical model for the optimal placement of piezoelectric plates to control the multimode vibrations of a fixed cantilever beam In this paper the model has been extendet to a rotating cantilever beam. After a detailed description of the theoretical model, various combinations of bi-modal excitations are considered. The design of the optimal configurations, for different coupled modes, different relative contributions and for various angular velocities are reported. The validity of the proposed optimization technique has been confirmed by comparison between numerical results, obtained by FEM simulations, and theoretical findings. The usefulness of the model can be assessed in many real situations when the spectrum of the load excites more eigenmodes and the damping is necessary to improve the integrity of engineering structures, e.g. gas turbine blades, or increase their fatigue life. The proposed model allows to find, for every load spectrum, the optimal configuration of the piezoelectric plates to obtain the best performances in terms of vibrations amplitude reduction or power consumed. The application of the proposed methodology to the real gas turbine blades [34], with the inclusion of the torsional modes, and their response to an impulse load [35] will constitute the object of further contributions.

## V. APPENDIX

$$\begin{cases} \mathbf{M}_{1_{ij}} = \rho_b S_b \int_0^{L_b} \phi_i(x)\phi_j(x)dx \\ \mathbf{M}_{2_{ij}} = \rho_b I_b \int_0^{L_b} \phi_i^{II}(x)\phi_j(x)dx \end{cases}$$

$$\begin{cases} \mathbf{K}_{1_{ij}} = E_b I_b \int_0^{L_b} \phi_i^{IV}(x)\phi_j(x)dx \\ \mathbf{K}_{2_{ij}} = E_b S_b \int_0^{L_b} u^{II}(x)\phi_i^{I}(x)\phi_j(x)dx \\ \mathbf{K}_{3_{ij}} = E_b S_b \int_0^{L_b} u^{I}(x)\phi_i^{II}(x)\phi_j(x)dx \end{cases}$$

## REFERENCES


[1] E. Poursaeidi and M. Salavatian, "Fatigue grow simulation in a generator fan blade," *Engineering Failure Analysis* vol. 16 pp. 888-898, 2009.

[2] L. Witek, "Experimental crack propagation and failure analysis of the first stage compressor blade subject to vibration," *Engineering Failure Analysis* 16 (7) pp. 2163-2170, 2009.

[3] J .Kubiac Sz., B. Urquiza G., J. Garci C. and F. Sierra E., "Failure analysis of steam turbine last stage blade tenon and shroud," *Engineering Failure Analysis* vol. 14 (8) pp. 1476-1487, 2007.

[4] E.F. Crawley, J. de Luis, J, "Use of piezoelectric actuators as elements of intelligent structures" *AIAA Journal* vol. 25, 1373-1385, 1987.

[5] A. Hohl, M. Neubauer, S. M. Schwarzendahl , L. Panning and J. Wallaschek, "Active and semiactive Vibration Damping of Turbine Blades with Piezoceramics," in *Proc. of SPIE*, 2009, Vol. 7288 72881H1-72881H10.

[6] I. Goltz, H. Bhmer, R. Nollau, J. Belz, B. Grueber and J. R. Seume, "Piezo-electric actuation of rotor blades in an axial compressor with Piezoceramics," in *Proc. of 8th European Conference on Turbomachinery (ETC)*, 23-27 March 2009, Graz, Austria.

[7] A. J. Provenza and C. R. Morrison, "Control of fan blade vibrations using piezoelectric and bi-directional telemetry," in *Proc. of ASME Turbo Expo*, 2011, June 6-10, 2011, Vancouver, British Columbia, Canada

[8] S. M. Schwarzendahl, "On blade damping technology using passive piezoelectric dampers," in *Proc. of ASME Turbo Expo*, 2012, June 11-15, 2012, Copenaghen, Denmark.

[9] B. Choi, J. Kauffman, K. Duffy, A. Provenza A. and C. Morrison, "Active Vibration Reduction of Titanium Alloy Fan Blades (FAN1) Using Piezoelectric Materials," *Propulsion-Safety and Affordable Readiness (P SAR) Conference cosponsored by U.S. Army, Navy, and Air Force*, 2010, Jacksonville, Florida, March 16/18.

[10] B. Choi, C. Morrison and K. Duffy, "An Active Damping at Blade Resonances Using Piezoelectric Transducers," *Propulsion-Safety and Affordable Readiness (PSAR) Conference cosponsored by the U.S. Army, Navy, and Air Force*, 2008, Myrtle Beach, South Carolina, March 18/ 20.

[11] M. I. Frecker, "Recent Advances in Optimization of Smart Structures and Actuators," *Journal of Intelligent Material System and Structures* vol. 14, pp. 207-216, 2003.

[12] V. Gupta,M. Sharma and T. Nagesh, "Optimization Criteria for Optimal Placement of Piezoelectric Sensors and Actuators on a Smart Structure: A Technical Review" *Journal of Intelligent Material Systems and Structures*, vol. 21, no. 12, pp. 1227-1243, 2010.

[13] K. D. Dhuri and P. Seshu "Piezo actuator placement and sizing for good control effectiveness and minimal change in original system dynamics," *Smart Materials and Structures* vol. 15, pp. 1661-1672, 2006.
[14] K Ramesh Kumar and S Narayanan, "Active vibration control of beams with optimal placement of piezoelectric sensor/actuator pairs" Smart Materials and Structures vol.17, no.5, pp. 1-15, 2008.
[15] M. Sunar and S. S. Rao, "Distributed Modeling and Actuator Location for Piezoelectric Control System," *AIAA Journal* vol. 34 no. 10 pp. 2209-2211, Oct. 1996.
[16] Demetriou. A Numerical Algorithm for the Optimal Placement of Actuators and Sensors for Flexible Structures. *Proc. of the American Control Conference*, Chicago, 2000, Illinois, p. 2290-2294.
[17] I. Bruant, G. Coffignal, F. Lene and M. Verge, "A methodology for determination of piezoelectric actuator and sensor location on beam structures," *Journal of Sound and Vibration* vol. 245 no. 5, pp. 861-882, 2001.
[18] A .Baz and S. Poh, "Performance of an active control system with piezoelectric actuators," *Journal of Sound and Vibration* vol. 126 no. 2 pp. 327-343, 1988.
[19] S. M. Yang, and Y. J. Lee, "Optimization of non-collocated sensor/actuator location and feedback gain in control systems," *Smart Materials and Structures* vol. 2, pp. 96-102, 1993.
[20] S. M. Yang, and Y. J. Lee, "Vibration suppression with optimal sensor/actuator location and feedback gain.," *Smart Materials and Structures* vol. 2, pp. 232-239, 1993.
[21] Y. Yang, J. Zhanli and C. K. Soh, "Integrated optimal design of vibration control system for smart beams using genetic algorithms," *Journal of Sound and Vibration* vol. 119, no. 3, pp. 487-508, 2005.
[22] R. Barboni, A. Mannini, E. Fantini and P. Gaudenzi, "Optimal placement of PZT actuators for the control of beam dynamics" *Smart Materials and Structures* Vol. 9, pp. 110–120, 2000.
[23] Q. Wang and C. M. Wang, "Optimal placement and size of piezoelectric patches on beams from the controllability perspective," *Smart Materials and Structures* vol. 9 pp. 558-567, 2000.
[24] F. Botta, Dini D., Schwingshackl C., di Mare L., Cerri G., "Optimal placement of piezoelectric plates to control multimode vibrations of a beam," *Advances in Acoustics and Vibration*, vol. 2013 (in press).
[25] F. Botta, N. Marx, S. Gentili, C. W. Schwingshackl, L. Di Mare L., G. Cerri, D. Dini, "Optimal placement of piezoelectric plates for active vibration control of gas turbine blades: experimental results," in Proc. of SPIE Vol. 8345, 2012, 83452H-183452H-11.
[26] F. Botta, N. Marx, D. Dini , R. de Lieto Vollaro and G. Battista, "Experimental results for optimal placement of piezoelectric plates for active vibration control of a cantilever beam," *International Journal of Engineering and Technology*, vol. 5, issue 5, October 2013.
[27] F. Botta, N. Marx, C. W. Schwingshackl, G. Cerri, D. Dini, "A wireless vibration control technique for gas turbine blades using piezoelectric plates and contactless energy transfer," in *Proc. of the ASME Turbo Expo*, 2013, June 3-7, San Antonio, Texas, USA.
[28] N. Marx, "Counter vibration on gas turbine compressor blades via piezoelectric plates," Master of Science Degree, Imperial College, London, 2012.
[29] F. Botta, G. Cerri, "Wave propagation in Reissner-Mindlin piezoelectric coupled cylinder with non-constant electric field through the thickness," *International Journal of Solids and Structures*, vol. 44, Issues 18-19, pp. 6201-6219, September 2007.
[30] J. C. Simo, "The role of non-linear theories in transient dynamic analysis of flexible structures," *Journal of Sound and Vibration* vol. 119 no. 3, pp. 487-508, 1987.
[31] G. Wang and N. M. Wereley, "Free Vibration Analysis of Rotating Blades with Uniform Tapers," *AIAA Journal* vol. 42, no. 12, pp. 2429-2437, 2004.
[32] S. M. Lin and J. M. Lin, "Vibration of Rotating Smart Beam," AIAA Journal vol. 45, no. 2, pp. 382-389, 2007.
[33] H. H. Yoo and S. H. Shin, "Vibration analysis of rotating cantilever beams," *Journal of Sound and Vibration*, vol. 212, no. 5, pp. 807-828, 1998.
[34] G. Cerri, M. Gazzino, F. Botta, C. Salvini, "Production Planning with Hot Section Life Prediction for Optimum Gas Turbine Management," *International Journal of Gas Turbine, Propulsion and Power Systems*, vol. 2, no. 1, pp. 9-16, 2008.
[35] F. Botta, G. Cerri, "Shock response spectrum in plates under impulse loads," *Journal of Sound and Vibration*, vol. 308, Issues 3-5, pp. 563-578, 4 December 2007.